Growth and photoluminescence properties of inclined ZnO and ZnCoO thin films on $SrTiO_3$(110) substrates*

Bai Hong-Liang(白洪亮), Liu Guo-Lei(刘国磊)†, He Shu-Min(贺树敏), Yan Shi-Shen(颜世申), Zhu Da-Peng(朱大鹏), Guo Hong-Yu(郭红雨), Ji Zi-Wu(冀子武), Yang Feng-Fan(杨丰帆), Chen Yan-Xue(陈延学), and Mei Liang-Mo(梅良模)

School of Physics and National Key Laboratory of Crystal Materials, Shandong University, Jinan 250100*, China*

(Received 21 December 2011; revised manuscript received 17 February 2012)

ZnO thin film growth prefers different orientations on the etched and unetched $SrTiO_3$(STO)(110) substrates. Inclined ZnO and cobalt-doped ZnO (ZnCoO) thin films are grown on unetched STO(110) substrates using oxygen plasma assisted molecular beam epitaxy, with the *c*-axis 42° inclined from the normal STO(110) surface. The growth geometries are ZnCoO[100]//STO[1$\bar{1}$0] and ZnCoO[1$\bar{1}$1]//STO[001]. The low temperature photoluminescence spectra of the inclined ZnO and ZnCoO films are dominated by D^0X emissions associated with A^0X emissions, and the characteristic emissions for the $^2E(^2G)\rightarrow{}^4A_2(^4F)$ transition of Co^{2+} dopants and the relevant phonon-participated emissions are observed in the ZnCoO film, indicating the incorporation of Co^{2+} ions at the lattice positions of the Zn^{2+} ions. The *c*-axis inclined ZnCoO film shows ferromagnetic properties at room temperature.

Keywords: inclined ZnO, $SrTiO_3$(110), photoluminescence

PACS: 78.55.–m, 81.15.–z, 81.20.–n **DOI:** 10.1088/1674-1056/21/5/057801

1. Introduction

As a wide bandgap oxide semiconductor, ZnO has a wide range of applications in gas sensors,[1] transparent coatings for solar cells,[2] and acoustic devices.[3] Recently, ZnO has attracted considerable attention in ultraviolet light emitting devices,[4−6] and ZnO-based spintronic devices.[7,8] In general, wurtzite structural ZnO shows a *c*-plane preferred growth because of its small surface energy compared with that of other crystal planes. However, the electrostatic field along the *c* axis from the spontaneous polarization and the piezoelectric polarization will cause a decrease in the inner quantum efficiency of the emitting device.[9,10] So much effort[11,12] has been devoted to nonpolar ZnO film growth, such as ZnO(110) and (100), to avoid the effects of the built-in electric field along the *c* axis.

Other than polar and nonpolar ZnO films, inclined ZnO films, with the *c*-axis tilted against the normal surface by an α ($0° < \alpha < 90°$) angle, have also been studied due to possible applications in piezoelectric shear wave transducers and anisotropic property studies.[13−15] To obtain inclined ZnO films, tilted Si wafers and miscut $SrTiO_3$ (STO) substrates are used for the DC magnetron sputtering[7,14] and pulsed laser deposition,[14] respectively. On the other hand, STO is an excellent perovskite substrate for functional oxide electronics, and a representative perovskite material.[16] The integration of ZnO and STO may open the way to fabricating wurtzite/perovskite multistructure devices and providing novel functional devices. Some efforts have been made to grow ZnO on the different planes of STO, such as STO (100), (110) and (111), [11,14,17,18] and polar and nonpolar ZnO films were obtained, while the inclined ZnO film was seldom obtained on STO substrates, and the sole report dealing with an inclined ZnO with twinned structure on STO(110) substrates is in Ref. [14]. We found that the selective etching process for STO(110) substrates significantly influences the growth orientation of ZnO thin films. In this work, we report on the growth and photoluminescence properties of *c*-axis inclined ZnO and cobalt-doped ZnO (ZnCoO) films grown on STO(110) single crystal substrates by radio frequency oxygen plasma assisted molecular beam epitaxy. The magnetic properties and the d–d transition-related photoluminescence properties for the inclined ZnCoO thin films are also investigated.

*Project supported by the National Basic Research Program of China (Grant No. 2009CB929202) and the National Natural Science Foundation of China (Grant Nos. 10834001 and 51125004).

†Corresponding author. E-mail: liu-guolei@sdu.edu.cn

© 2012 Chinese Physical Society and IOP Publishing Ltd

2. Experiments

ZnO and ZnCoO thin films were grown on commercial STO(110) substrates by radio frequency oxygen plasma assisted molecular beam epitaxy (OPAMBE). We found that the growth of ZnO thin films preferred different orientations on the etched and unetched STO(110) substrates. Based on this, three typical samples were selected to reveal the detailed growth properties and the optical properties: 1) sample A is ZnO (410 nm) on etched STO(110), 2) sample B is ZnO (240 nm) on unetched STO(110), and 3) sample C is ZnCoO (220 nm) on unetched STO(110). For sample A, its substrate was pre-etched in NH_3 buffered HF solution (BHF) (pH≈4.5) for 2 min. To clean possible carbonic contamination, annealing was applied to all STO(110) substrates at 800 °C for 20 min in an ultra-high vacuum chamber. These films were grown at 450 °C under oxygen partial pressure 3×10^{-4} Pa. High pure Zn(6N) and Co(4N) solid sources were co-evaporated from the *k*-cells. The fluxes of Zn and Co were manipulated by a quartz microbalance, and cross-checked by *in situ* X-ray photoelectron spectroscopy and *ex situ* energy dispersive X-ray fluorescence analysis. The whole growth process was monitored by reflection high energy electron diffraction (RHEED). The crystal structure was characterized by high resolution X-ray diffraction (HRXRD, Bruker AXS), and the photoluminescence (PL) spectra were excited by a 325 nm He–Cd laser and collected with an iHR 320 imaging spectrometer (HORIBA Jobin Yvon Inc.) equipped with a CCD detector. The magnetism was measured by an alternative gradient magnetometer (AGM).

3. Results and discussion

Figure 1 shows the XRD θ–2θ scans for samples A, B and C. The diffraction peaks of both the ZnO(002) and (102) peaks match well with the corresponding lattice constant of wurtzite ZnO. The *c*-axis oriented ZnO and *c*-axis inclined ZnO coexist in the same sample, while the ZnO(002) peak is predominant for sample A, and the ZnO(102) peak is predominant for sample B. The ZnCoO film of sample C shows the same orientation as that of sample B.

The growth geometries for the *c*-axis inclined (samples B and C) and *c*-axis orientation (sample A) ZnO and ZnCoO films were determined by XRD θ–2θ scans combined with XRD φ scans. Figure 2(a) shows the XRD φ scans of the (002) plane of inclined ZnCoO patches in sample C, and with respect to the STO(100) and (111) planes. χ is the rotating angle of the *c*-axis from the normal STO(110) surface. According to XRD φ scans, we can figure out the in-plane relationship between the inclined ZnCoO patches and STO(110): ZnCoO[100]//STO[1$\bar{1}$0] and ZnCoO [1$\bar{1}$1]//STO [001]. The schematic drawings are illustrated in Figs. 2(c) and 2(d). Its *c*-axis is 42° inclined against the normal STO(110) surface. It is notable that there is only one peak for the (002) plane of the inclined ZnCoO patches in the φ scan, indicating a mono-orientation. Furthermore, the full width at half maximum (FWHM) of the ZnCoO(102) peak is 0.20°, indicating a good crystalline structure, as shown in the XRD rocking curve in Fig. 2(b). The sharp XRD rocking curve and φ scans indicate that the inclined ZnCoO patches are well oriented and no twinned symmetry is observed in our samples, which is in contrast to the twinned ZnO/STO(110) prepared using other methods.[14] The in-plane strains for inclined ZnCoO patches are anisotropic, and different tensile strains are present with respect to the STO[001] and [1$\bar{1}$0] directions, respectively, as shown in Fig. 2(c). The lattice mismatch along the STO[001] direction is −1.7% with two STO units ($2a_{\rm STO}$ = 0.781 nm) matching the diagonal distance ($\sqrt{3a_{\rm ZnO}^2 + c_{\rm ZnO}^2}$ ≈ 0.768 nm) of ZnO along the ZnO[1$\bar{1}$1] direction. The lattice mismatch along the STO[1$\bar{1}$0] direction is −11.7% with three ZnO units ($3a_{\rm ZnO}$ ≈ 0.975 nm) matching two diagonal distances $(2(2)^{1/2}a_{\rm STO}$≈ 1.104 nm) of STO(110) along the STO[1$\bar{1}$0] direction.

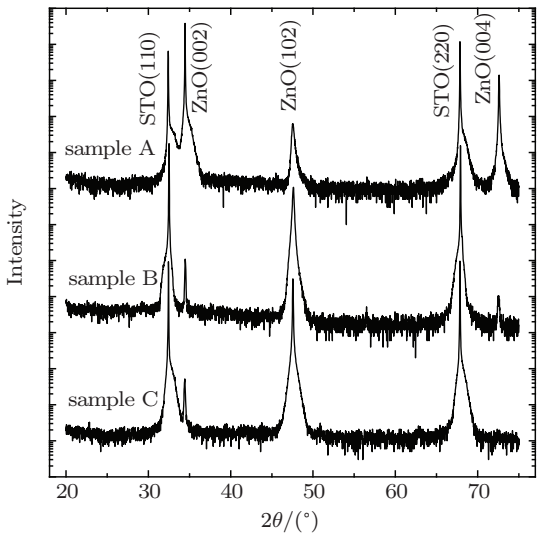


Fig. 1. XRD θ–2θ scans for samples A, B and C.

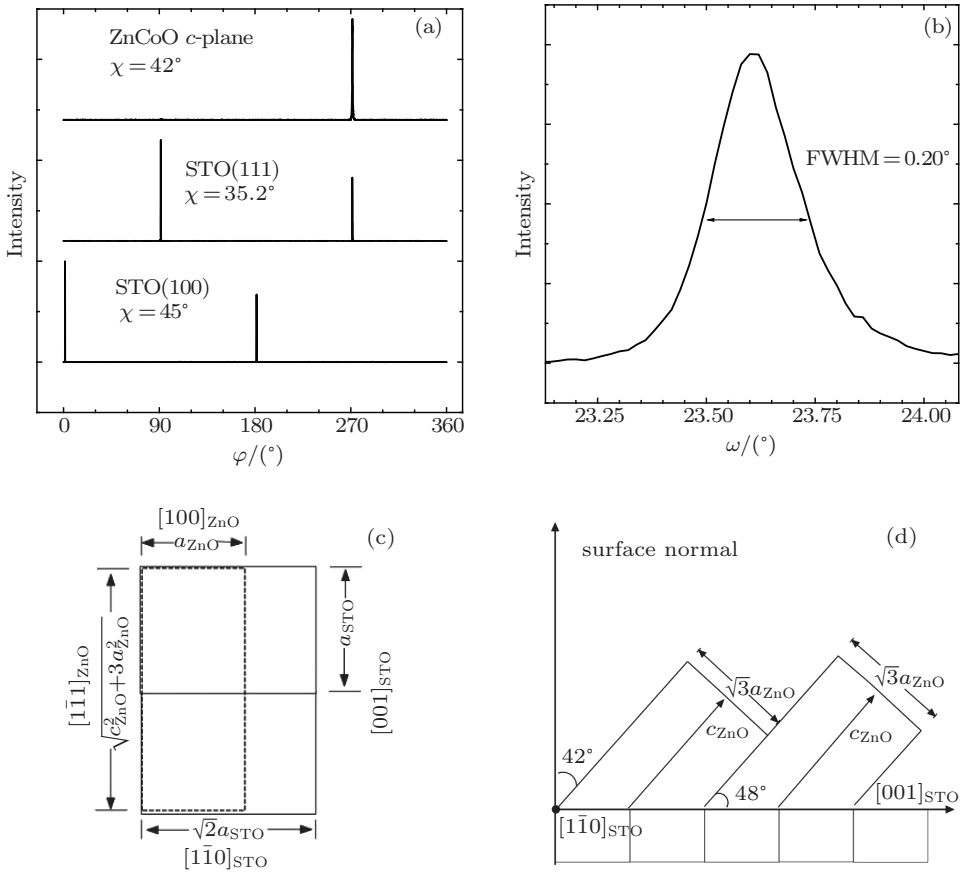


Fig. 2. (a) XRD φ scans of the ZnCoO(002) plane with respect to those of the STO(111) and STO(100) planes. (b) The rocking curve of the ZnCoO(102) peak for the c-axis inclined ZnCoO patches. (c and d) Schematic drawing of the epitaxial relationship between the inclined ZnCoO patches and the STO(110) substrate from (c) the top view and (d) the side view.

Similarly, we can determine the in-plane relationships of the c-axis orientation ZnO on STO(110) (sample A): ZnO[100]//STO[001] and ZnO[1$\bar{1}$0]//STO[1$\bar{1}$0], which are consistent with the experimental results reported by other groups.[11,18] The in-plane strains for c-axis orientation ZnO are also anisotropic. Compressed strain is present with respect to the STO[1$\bar{1}$0] direction with a lattice mismatch of +1.9% and tensile strain is present with respect to STO[001] direction with a lattice mismatch of −16.8%.

As in the above discussion, c-axis inclined ZnO prefers to grow on unetched STO(110), while c-axis orientation ZnO prefers to grow on etched STO(110). Considering the same deposition process for the three samples, except the pretreatment of the substrates, we can find that the preferred growth orientation is mainly affected by selective etching to the surface of the STO(110) substrates. For $SrTiO_3$, the strontium ions are much easier to dissolve in acid solution than titanium ions.[19] Thus, the STO(110) surface prefers to be TiO_x terminated after etching in BHF, while the surface of the polished unetched STO(110) remains mixed SrO_y and TiO_x. The selective etching process will greatly change the surface conditions of the STO(110) face, such as terminated bonding, surface charge, etc, which possibly causes the discrepancy of the preferred growth orientations of subsequent ZnO films.

Figure 3 shows the PL spectra for samples A, B, and C at 5.8 K. The PL spectra near the band edge are dominated by the recombination of exciton bound to neutral donor (D^0X) as shown in Fig. 3(a). The satellite emissions at 3.319 eV present, respectively, at samples B and C, can both be assigned to the recombination of exciton bound to neutral acceptor (A^0X).[20−22] The emissions at 3.243 eV appear, respectively, for samples B and C, and both of them can be assigned to donor-acceptor-pair transition (DAP). It is notable that the A^0X emissions are easy to observe for samples B and C with c-axis inclined ZnO patches, and the A^0X emission is absent for sample A with c-axis orientation ZnO patches. The longitudinal optical (LO) phonon replica for D^0X and DAP are labeled as (D^0X-nLO) and (DAP-nLO), respectively, with an energy interval ∼ 72 meV, where n is

the number of phonons emitted in the transition.

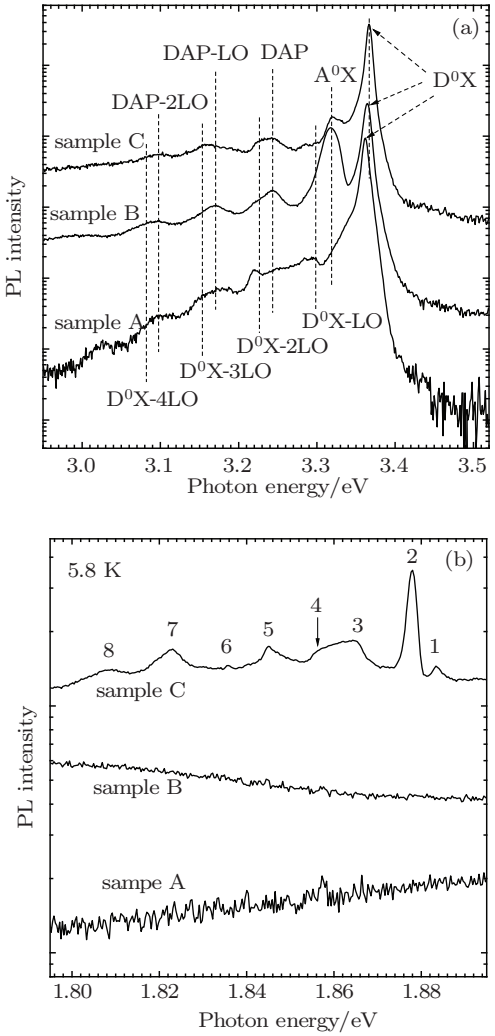


Fig. 3. PL spectra of samples A, B, and C at 5.8 K (a) near the band edge and (b) in the Co^{2+} ion related d–d transition region (red region) near 1.87 eV.

Table 1. Characteristic emissions of the PL spectrum for sample C in the red region at 5.8 K. Emissions #1 and #2 are from the Co^{2+} d–d transitions of $^2E(G)_{3/2} \rightarrow {}^4A_2(^4F)$ and $^2E(G)_{1/2} \rightarrow {}^4A_2(^4F)$, respectively. The emissions from #3 to #8 (except #6) are the phonon replicas of emission #2, and #6 is the phonon replica of emission #1. ΔE is the energy interval corresponding to #2 (ZPL). $E_2{}^{low}$, $E_2{}^{high}$, LA, LO, A_1(TO) and A_1(LO) denote the Raman vibration modes in bulk ZnO.[23,24]

Emission	energy/eV	ΔE/meV	Identification
#1	1.883	−5	$^2E(G)_{3/2} \rightarrow {}^4A_2(^4F)$
#2	1.878	0	ZPL,$^2E(G)_{1/2} \rightarrow {}^4A_2(^4F)$
#3	1.865	13	ZPL-$E_2{}^{low}$
#4	1.856	22	ZPL-LA[A] or/and ZPL-LO[A]
#5	1.845	33	ZPL-$B_1{}^{low}$
#6	1.836	47 − 5	#1-A_1(TO)
#7	1.823	55	ZPL-$E_2{}^{high}$
#8	1.809	69	ZPL-A_1(LO)

Figure 3(b) shows the PL spectra in the red region at 5.8 K. Eight characteristic emissions at ∼ 1.87 eV are observed for the Co-doped ZnO film, while these emissions are absent for undoped ZnO films. Emission #2 at 1.878 eV is attributed to the direct transition between the $^2E(G)_{1/2}$ state and the $^4A_2(^4F)$ ground state of Co^{2+} ions under the tetrahedral crystal field formed by neighbouring O^{2-} ions within the ZnO wurtzite structure.[25,26] Since there is no participating phonon, emission #2 is referred to as the zero phonon line (ZPL). The energy interval between #1 and #2 is 4.7 meV, and matches the energy interval between the $^2E(G)_{3/2}$ and $^2E(G)_{1/2}$ states, which comes from the splitting states of $^2E(^2G)$ due to spin-orbit coupling.[25,27] So emission #1 is attributed to the transition from the $^2E(G)_{3/2}$ state to the ground state $^4A_2(^4F)$. The emissions from #3 to #8 (except #6) can be assigned to the transition of $^2E(G)_{1/2} \rightarrow {}^4A_2(^4F)$ combined with the phonons from the ZnO lattice. They can be assigned to the phonon replicas of emission #2, and emission #6 can be assigned to the phonon replica of emission #1. Their spectral positions and the values of energy interval E with respect to ZPL #2 are listed in Table 1. The participating phonon modes can be assigned by the vibration modes in bulk ZnO.[23,24] For example, the energy interval between #7 and #2 is 55 meV, which accords well with the energy of the $E_2{}^{high}$ mode (54 meV). The presence of characteristic emissions near 1.87 eV indicates the incorporation of Co^{2+} ions at the lattice positions of the Zn^{2+} ions in sample C.

Ferromagnetism is observed for this *c*-axis inclined ZnO thin film doped with a slight number of Co^{2+} ions (∼4.2%), as shown in Fig. 4. A clear *M*–*H* hysteresis loop with small coercive field, ∼ 20 Oe (1 Oe=79.5775 A/m), is observed, indicating room temperature ferromagnetism. The saturation magnetization is 3.23 emu/cm^3 (0.2 μ_B/Co) (1 emu/cm^3=10^3 A/m), which is comparable to that (∼ 0.4 μ_B/Co with 4.9% Co^{2+} ions) of our previous ZnCoO film on a sapphire substrate,[28] and no clear anisotropy is observed. It seems that the saturation magnetization is not sensitive to the asymmetric strains in our inclined ZnCoO film. Similarly, the room temperature ferromagnetism can also be explained as the percolation of bound magnetic polarons.[29,30]

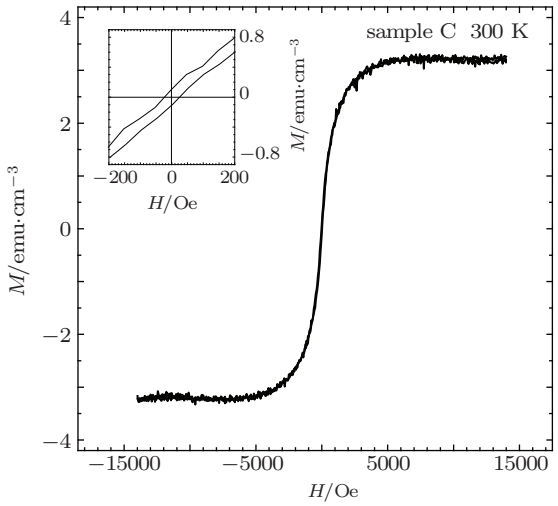


Fig. 4. M–H curve for sample C at room temperature. The inset shows the details in the low field region.

4. Conclusion

In the present paper, ZnO and ZnCoO thin films are grown on STO(110) substrates by OPAMBE. In the same ZnO film, two competing growth orientations are present and modulated by a selective etching process to the surface of the STO(110) substrates. The c-axis orientated ZnO patches prefer to grow on STO(110) etched by BHF solution with a TiO_x-terminated surface, while the c-axis inclined ZnO patches prefer to grow on unetched STO(110) with a terminated surface of mixed SrO_y and TO_x. For the inclined ZnO and ZnCoO patches, the c-axis is 42° inclined from the normal STO(110) surface without a twinned structure, and the in-plane relationships between the film and substrate are ZnCoO[100]//STO[1$\bar{1}$0] and ZnCoO[1$\bar{1}$1]//STO[001]. Their PL spectra are dominated by D^0X emissions associated with an A^0X emission. For the ZnCoO film, several characteristic emissions from the $^2E(^2G)\rightarrow{}^4A_2(^4F)$ transition are observed, indicating the incorporation of Co^{2+} ions at the lattice positions of Zn^{2+} ions. The ZnCoO film shows ferromagnetism at room temperature.

References

[1] Cheng X L, Zhao H, Huo L H, Gao S and Zhao J G 2004 *Sensor Actuat. B-Chem.* **102** 248

[2] Manna U, Yoo J, Dhungel S K, Gowtham M, Gangopadhyay U, Kim K, Yi J and Saha H 2005 *J. Korean Phys. Soc.* **46** 1378

[3] Yan Z, Song Z, Liu W, Ren H, Gu N, Zhou X, Zhang L, Wang Y, Feng S, Lai L and Chen J 2007 *Appl. Surf. Sci.* **253** 9372

[4] Tsukazaki A, Ohtomo A, Onuma T, Ohtani M, Makino T, Sumiya M, Ohtani K, Chichibu S F, Fuke S, Segawa Y, Ohno H, Koinuma H and Kawasaki M 2005 *Nat. Mater.* **4** 42

[5] Su S C, Lu Y M and Mei T 2011 *Acta Phys. Sin.* **60** 096801 (in Chinese)

[6] Li M, Zhang H Y, Guo C X, Xu J B, Fu X J and Chen P F 2009 *Chin. Phys.* B **18** 5020

[7] Wolf S A, Awschalom D D, Buhrman R A, Daughton J M, Von Molnár S, Roukes M L, Chtchelkanova A Y and Treger D M 2001 *Science* **294** 1488

[8] Ohno H 1998 *Science* **281** 951

[9] Wetzel C, Takeuchi T, Amano H and Akasaki I 2000 *Phys. Rev.* B **62** R13302

[10] Park S H and Ahn D 2005 *Appl. Phys. Lett.* **87** 253509

[11] Wei X H, Li Y R, Zhu J, Huang W, Zhang Y, Luo W B and Ji H 2007 *Appl. Phys. Lett.* **90** 151918

[12] Zhang Y, Li X, Yu W, Yang C, Cao X, Gao X, Kong J, Shen W, Zhao J and Sun X 2009 *J. Phys.* D. *Appl. Phys.* **42** 075410

[13] Wang J S and Lakin K M 1983 *Appl. Phys. Lett.* **42** 352

[14] Peruzzi M, Pedarnig J D, Bäuerle D, Schwinger W and Schäffler F 2004 *Appl. Phys.* A **79** 1873

[15] Lee Y E, Kim S G, Kim Y J and Kim H J 1997 *J. Vac. Sci. Technol.* A **15** 1194

[16] Santander-Syro A F, Copie O, Kondo T, Fortuna F, Pailhes S, Weht R, Qiu X G, Bertran F, Nicolaou A, Taleb-Ibrahimi A, Le Fevre P, Herranz G, Bibes M, Reyren N, Apertet Y, Lecoeur P, Barthelemy A and Rozenberg M J 2011 *Nature* **469** 189

[17] Sugiura M, Nakashima Y, Nakasaka T and Kobayashi T 2002 *Appl. Surf. Sci.* **197** 472

[18] Kim D W, Shin S, Kim Y, Chang S H, Chang Y J, Kim M and Jeong H 2007 *Solid State Commun.* **143** 140

[19] Kawasaki M, Takahashi K, Maeda T, Tsuchiya R, Shinohara M, Ishiyama O, Yonezawa T, Yoshimoto M and Koinuma H 1994 *Science* **266** 1540

[20] Nam Y S, Lee S W, Baek K S, Chang S K, Song J H, Song J H, Han S K, Hong S K and Yao T 2008 *Appl. Phys. Lett.* **92** 201907

[21] Schirra M, Schneider R, Reiser A, Prinz G M, Feneberg M, Biskupek J, Kaiser U, Krill C E, Sauer R and Thonke K 2007 *Physica* B **401–402** 362

[22] Chi D H, Binh L T T, Binh N T, Khanh L D and Long N N 2006 *Appl. Surf. Sci.* **252** 2770

[23] Schulz H J and Thiede M 1987 *Phys. Rev.* B **35** 18

[24] Cuscó R, Alarcón Lladó E, Ibáñez J, Artús L, Jiménez J, Wang B and Callahan M J 2007 *Phys. Rev.* B **75** 165202

[25] Koidl P 1977 *Phys. Rev.* B **15** 2493

[26] Trinh Thi L, Nguyen Ngoc L and Le Hong H 2009 *J. Phys.* D. *Appl. Phys.* **42** 065412

[27] Weakliem H 1962 *J. Chem. Phys.* **36** 2117

[28] Liu G L, Cao Q, Deng J X, Xing P F, Tian Y F, Chen Y X, Yan S S and Mei L M 2007 *Appl. Phys. Lett.* **90** 052504

[29] Coey J M D, Venkatesan M and Fitzgerald C B 2005 *Nat. Mater.* **4** 173

[30] Weng Z Z, Zhang J M, Huang Z G and Lin W X 2011 *Chin. Phys.* B **20** 027103